Hindawi
Journal of Engineering
Volume 2017, Article ID 6987265, 6 pages
https://doi.org/10.1155/2017/6987265

*Research Article*

# Numerical Simulation Modeling of Carbonate Reservoir Based on Rock Type

**Peiqing Lian, Cuiyu Ma, Bingyu Ji, Taizhong Duan, and Xuequn Tan**

*Sinopec Petroleum Exploration and Production Research Institute, Beijing, China*

Correspondence should be addressed to Peiqing Lian; lianpq.syky@sinopec.com

Received 18 May 2017; Revised 26 July 2017; Accepted 3 August 2017; Published 1 November 2017

Academic Editor: Yingfang Zhou



There are many types of carbonate reservoir rock spaces with complex shapes, and their primary pore structure changes dramatically. In order to describe the heterogeneity of K carbonate reservoir, equations of porosity, permeability and pore throat radii under different mercury injection saturations are fitted, and it shows that 30% is the best percentile. $R_{30}$ method is presented for rock typing, and six rock types are divided according to $R_{30}$ value of plugs. The porosity-permeability relationship is established for each rock type, and their relevant flow characteristics of each rock type have been studied. Logs are utilized to predict rock types of noncored wells, and a three-dimensional (3D) rock type model has been established based on the well rock type curves and the sedimentary facies constraint. Based on the relationship between $J$ function and water saturation, the formula of water saturation, porosity, permeability, and oil column height can be obtained by multiple regressions for each rock type. Then, the water saturation is calculated for each grid, and a 3D water saturation model is established. The model can reflect the formation heterogeneity and the fluid distribution, and its accuracy is verified by the history matching.

## 1. Introduction

$K$ reservoir is a large carbonate reservoir, the storage space is dominated by secondary interstices and vugs, and there are few fractures. $K$ reservoir buried depth is very deep and is affected by the strong diagnosis. Its primary pore structure changes dramatically, and the reservoir physical property distribution has strong heterogeneity. Rock typing is an essential step in the process of the carbonate reservoir characterization and geological modeling, and it is the method of classifying reservoir rocks which have the same fluid flow features into groups [1–6]. Rock typing is an effective way to obtain accurate permeability, and it enables us to get better understanding of the fluid movement and to enhance oil recovery [7–11].

There are several well-known models for the rock type discrimination. Leverett introduced the famous $J$ Function which could be used for rock typing [12, 13]. Winland [14] used the mercury injection-capillary pressure curves to develop an empirical relationship among porosity, permeability, and pore throat radii to different mercury saturations and found that the 35th percentile gave the best correlation. Amaefule et al. [15, 16] introduced a hydraulic flow unit concept and developed a method to predict the permeability of cored and uncored intervals; they grouped different rock samples based on their pore attributes similarity.

In this paper, we focus on the high heterogeneity of $K$ reservoir and study the rock typing method for carbonate reservoirs. The capillary pressure curves and the relative permeability curves are assigned to each rock type, and different flow units are generated. Based on geological model, the numerical simulation model has been established, and the accuracy of the model is verified by the history production matching.

## 2. Rock Typing Method

Darcy's law is an equation that describes the flow of a fluid through porous medium. It can be expressed as follows:

$$q = \frac{KA_p}{\mu} \cdot \frac{\Delta P}{L_p}, \tag{1}$$

where $q$ is volumetric flow rate, $K$ is permeability, $A_p$ is cross-sectional area of plug, $\mu$ is viscosity, $L_p$ is length of plug, and $\Delta P$ is pressure drop.

Poiseuille's equation can be used to determine the pressure drop of a constant viscosity fluid exhibiting laminar flow through a rigid pipe.

$$q = \frac{n\pi r_i^4}{8\mu} \cdot \frac{\Delta P}{L_a}, \tag{2}$$

where $n$ is number of capillary tubes, $r_i$ is pore throat radius of $i$th tube, and $L_a$ is apparent length of fluid flow path.

For homogenous plug samples, porosity can be calculated by the following equation:

$$\varphi = \frac{n\pi r_i^2}{A_p} \cdot \frac{L_a}{L_p}, \tag{3}$$

where $\varphi$ is effective porosity.

By applying Darcy's and Poiseuille's Laws, a relationship between porosity and permeability can be derived as the following equation:

$$K = \frac{r_i^2 \varphi}{8\tau^2}, \tag{4}$$

where $\tau$ is tortuosity, $\tau = (L_a/L_p)^2$.

Converting (4) into logarithmic form, we can derive the following equation:

$$\log r_i = C + A \log K - B \log \varphi, \tag{5}$$

where $A$, $B$, and $C$ are constant parameters.

For $K$ reservoir, porosity, permeability, and mercury injection experiments have been carried out for 206 plugs, and the throat radii with the mercury saturation ranging from 10% to 85% are calculated for each plug. Taking $R_{10}$ (throat radius at the mercury saturation of 10%) as an example, each plug has a $R_{10}$ value, porosity, permeability, and $R_{10}$ of 206 plugs consist of three vectors. By adopting the multiple regression method, the coefficients of (5) can be fitted. Using the same method, the equations of porosity, permeability, and pore throat radii under different mercury injection saturations are fitted.

It is shown in Figure 1 that the radius at mercury saturation 30% has the best correlation with porosity and permeability.

The fitting equation at mercury injection saturation of 30% is

$$\log(R_{30}) = 0.611 + 0.509 \log(K) - 0.694 \log(\varphi), \tag{6}$$

Based on the pore throat distributions of plugs, we define five typical pore throat radii; they are separately 0.1$\mu$m, 0.3$\mu$m, 1.0$\mu$m, 3.0$\mu$m, and 10.0$\mu$m, and six rock types can be distinguished by five typical pore throat radii. As shown in Figure 2, five typical curves divide the points into six regions. The relationship between porosity and permeability of each region can be fitted, and the correlation coefficients of fitting equations are reasonably high.

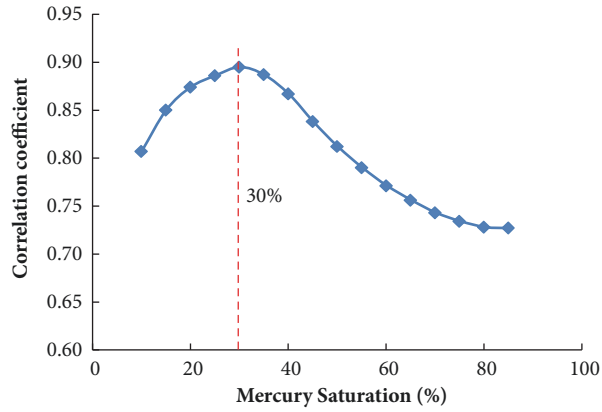


Figure 1: Correlation coefficients of fitting equations of porosity, permeability, and pore throat radii under different mercury injection saturations.

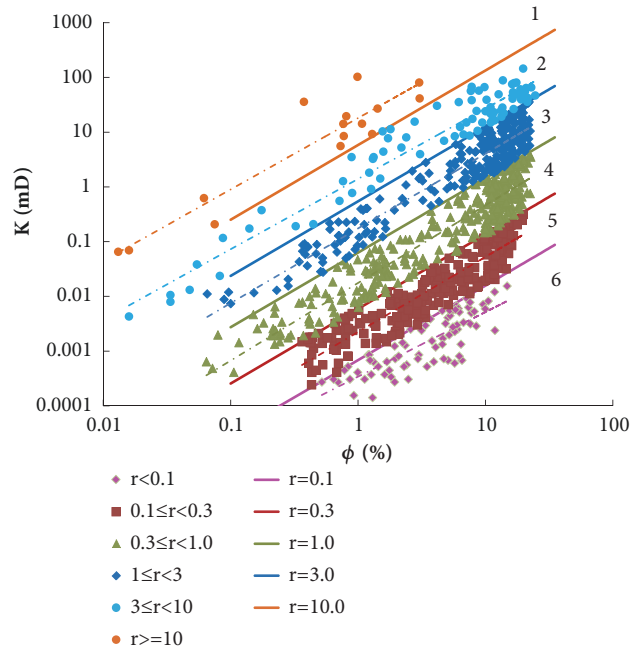


Figure 2: Rock type classification of $K$ reservoir.

(1) Rock type 1: $K = 19.076\varphi^{1.0431}$, $R^2 = 0.7341$

(2) Rock type 2: $K = 1.4015\varphi^{1.2853}$, $R^2 = 0.9334$

(3) Rock type 3: $K = 0.1749\varphi^{1.3659}$, $R^2 = 0.9021$

(4) Rock type 4: $K = 0.0176\varphi^{1.4183}$, $R^2 = 0.9011$

(5) Rock type 5: $K = 0.0022\varphi^{1.3722}$, $R^2 = 0.8569$

(6) Rock type 6: $K = 0.0004\varphi^{1.1005}$, $R^2 = 0.6858$

## 3. Flow Characteristics of Each Rock Type

*3.1. Capillary Pressure Curve of Each Rock Type.* Capillary pressure curve is useful in characterizing rock type, because

Table 1: Average porosity, average permeability, and J function for each rock type.

| Rock type | $K_{ave}$, mD | $\varphi_{ave}$, % | sqrt($K_{ave}/\varphi_{ave}$) | J function |
|---|---|---|---|---|
| 1 | 117.32 | 3.26 | 59.99 | $J = 0.1399S_{wn}^{-1.664}$ |
| 2 | 40.57 | 13.44 | 17.37 | $J = 0.1316S_{wn}^{-1.637}$ |
| 3 | 7.64 | 12.48 | 7.82 | $J = 0.0805S_{wn}^{-1.594}$ |
| 4 | 1.03 | 11.24 | 3.03 | $J = 0.0410S_{wn}^{-1.543}$ |
| 5 | 0.11 | 8.76 | 1.12 | $J = 0.0157S_{wn}^{-1.510}$ |

Table 2: Endpoint values of relative permeability curve of each rock type.

| Rock type | Swi | Kro@Swi | Sorw | krw @ Sorw |
|---|---|---|---|---|
| 1 | 0.33 | 0.69 | 0.41 | 0.42 |
| 2 | 0.20 | 0.65 | 0.31 | 0.31 |
| 3 | 0.23 | 0.59 | 0.33 | 0.28 |
| 4 | 0.26 | 0.55 | 0.35 | 0.25 |
| 5 | 0.30 | 0.52 | 0.38 | 0.20 |

it is an indication of pore throat distribution within one rock type. According to the principle of rock typing, the plugs are classified into six groups. Rock type 6 is very tight with low porosity; the fluid cannot flow in this rock type. Therefore, it could be regarded as a barrier.

We use $J$ function to make unique dimensionless drainage capillary pressure curves. For mixed-wet conditions, $J$ function does not work well because the value of permeability depends on the capillary pressure [17]. For $K$ reservoir, the average $J$ function value of each rock type is obtained by data regression.

$$J(S_{wn}) = \frac{P_{c,ave}}{\sigma \cos\theta} \cdot \sqrt{\frac{K_{ave}}{\varphi_{ave}}}, \quad (7)$$

$$S_{wn} = \frac{S_w - S_{wc}}{1 - S_{or} - S_{wc}}, \quad (8)$$

where $P_{c,ave}$, $K_{ave}$, and $\varphi_{ave}$ are average capillary pressure, permeability, and porosity of plugs under the same water saturation; $\sigma$ is interfacial tension; $\theta$ is wetting angle; $S_{wn}$ is normalized water saturation; $S_w$ is water saturation; $S_{wc}$ is connate water saturation; $S_{or}$ is irreducible oil saturation.

The average porosity, average permeability, and $J$ function for each rock type are shown in Table 1. An inverse transformation is performed on (7), and the capillary pressure curve of each rock type can be obtained. As shown in Figure 3, we can find that the capillary pressure curves have obvious regular rules except for rock type 1, and as the rock type number increases, the capillary pressure becomes higher under the same water saturation. The plugs of rock type 1 have fractures, it is easy for fluid to enter fractures, but it is difficult to enter matrix; therefore, the feature of capillary pressure curve is different from others.

*3.2. Relative Permeability Curve of Each Rock Type.* We have carried out relative permeability tests for 66 plugs; they cover from rock type 1 to rock type 5. Because of the heterogeneity of carbonate reservoir, we have not found any rules from the endpoint distributions of relative permeability curves, so we calculate the average value of each rock type, as shown in Table 2.

Corey saturation function is derived to fit the average relative permeability curves [18]. Based on the fit results and the average normalized relative permeability, the denormalized relative permeability curves are calculated and plotted for each rock type. As shown in Figure 4, the relative permeability curves show obvious regular rules except for rock type 1. As the rock type number increases, the irreducible water saturation increases, the two-phase flow region become narrow, and the relative permeability at isotonic point decreases. The plugs of rock type 1 have fractures, and the relative permeability curves have different characteristics.

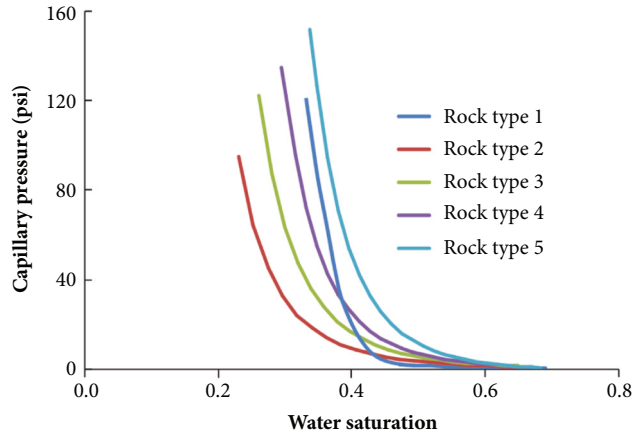


Figure 3: Capillary pressure curves of five rock types.

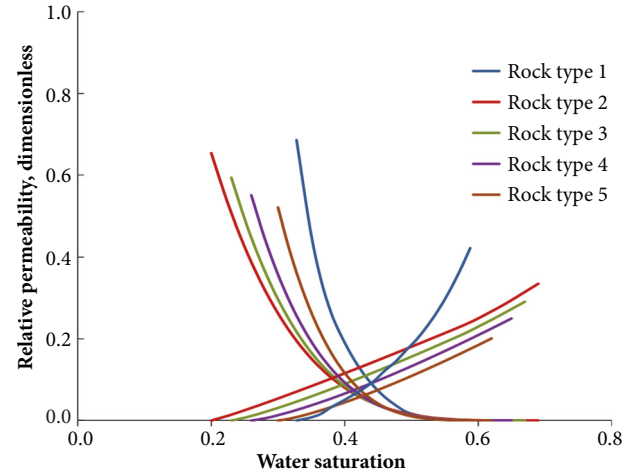


Figure 4: Relative permeability curves of five rock types.

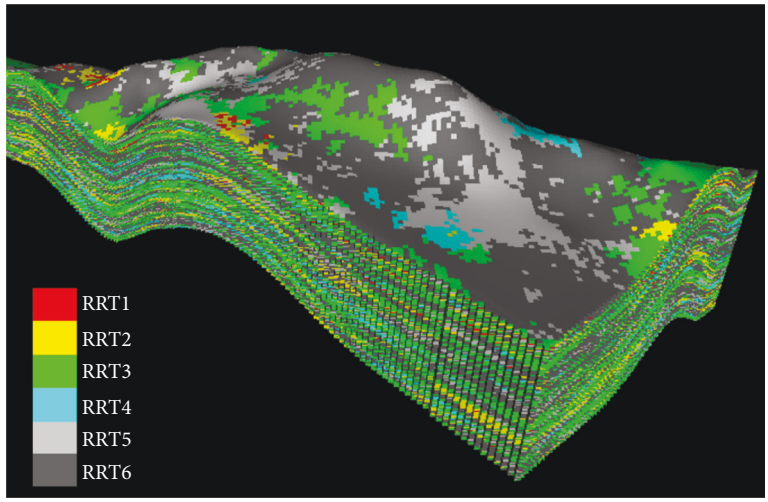


Figure 5: 3D rock type model.

## 4. Numerical Simulation Based on Rock Type

*4.1. 3D Rock Type Model.* Each plug has a coring depth, and we can find the logging data at corresponding depth. The rock type number and the logging data of each plug compose a sample. By using these samples, a link is set up between rock types and log responses by the KNN ($K$ Nearest Neighbor) method. Logs are utilized to predict rock types of noncored wells according to this link, and then the rock type curves of all wells can be obtained. Using this method, a 3D rock type model is established based on well rock type curves and sedimentary facies constraint, as shown in Figure 5.

The porosity model is built up based on logging data, seismic attribution, and sedimentary facies control. According to the relationship between porosity and permeability of each rock type, 3D permeability model can be established. The capillary pressure curve and the relative permeability curve are assigned to each rock type, and different flow units are generated.

*4.2. 3D Water Saturation Model.* The capillary pressure can be transformed into oil column height under formation conditions; (7) can be written into the following form:

$$J(S_{wn}) = \frac{(H_{owc} - H)(\rho_w - \rho_o)\, g}{\sigma \cos\theta} \cdot \sqrt{\frac{K_{ave}}{\varphi_{ave}}}, \quad (9)$$

where $H_{owc}$ is the depth of water/oil contact; $H$ is the height of arbitrary point in transition zone; $\rho_w$ and $\rho_o$ are the density of water and oil; $g$ is the acceleration of gravity.

According to (9), water saturation, porosity, permeability, and oil column height relationship can be obtained by multiple regressions. The oil column height can be calculated based on the depth difference between water/oil contact and grid depth, and the water saturation is calculated for each grid. There are different $J$ functions for different rock types; with the changes of the physical properties of formation, water saturation will show different characteristics.

*4.3. History Performance Matching.* As the numerical simulation model has been established, we have to testify the accuracy of the model. We use fixed oil production rate as the inner boundary condition, and the actual production process of the simulation area has been reappeared by the history matching. The fitting rates of the daily oil production rate and water cut are up to 99.8% and 93.6%.

Taking wells K2 and K8 as an example (their formation thickness is similar), we calculate the thickness proportion of different rock types of these two wells. As shown in Figure 6, rock types 4 and 5 are the main types for the well K2, and for K8, rock types 2 and 3 are the main. The reservoir property near K8 is better than that of K2, and the daily production rate of K8 is much higher than that of K2. This proves that the rock type classification is in coincidence with the production performance, and the model is reliable for the further design of the development plan.

## 5. Conclusions

(1) By applying Darcy's and Poiseuille's Laws, the relationships among porosity, permeability, and different pore throat radii have been fitted, and the typical pore throat radius $R_{30}$ has been selected.

(2) $R_{30}$ method is presented to define six petrophysical rock types with different reservoir properties. The capillary pressure curves and the relative permeability curves are assigned to each rock type, and difference flow units are generated.

(3) Based on geological model, the numerical simulation model has been established, and it can reflect the heterogeneity and the fluid distribution of formation very well and can be used to design the further development plan.

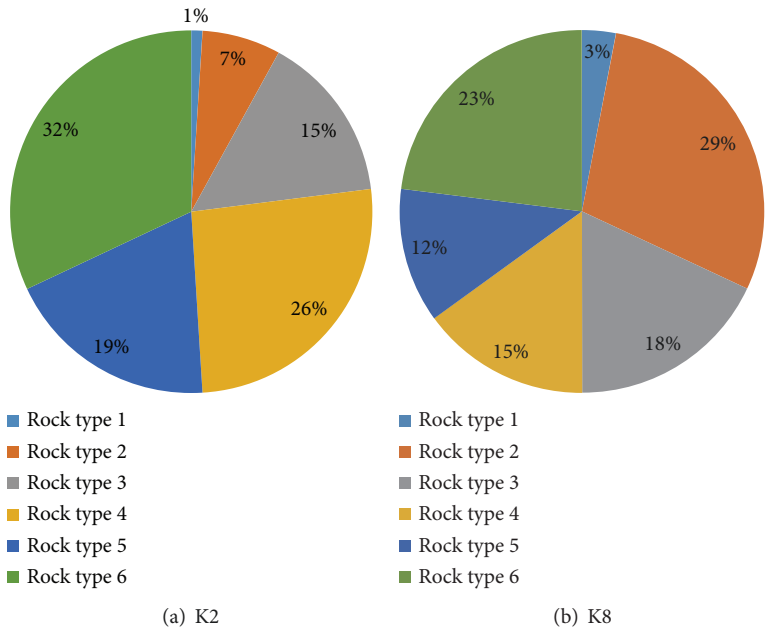


Figure 6: The thickness proportion of different rock types of wells K2 and K8.

## Conflicts of Interest

The authors declare that they have no conflicts of interest.

## Acknowledgments

The authors are grateful for the financial support from the National Science & Technology Major Projects of China (Grant no. 2016ZX05033-003), the National Science Fund for Young Scholars of China (Grant no. 41702359), and the Corporate Science & Technology Projects of Sinopec (Grant no. P15129).

## References

[1] M. R. Dernaika, B. Mansour, D. Gonzalez et al., "Upscaled Permeability and Rock Types in a Heterogeneous Carbonate Core from the Middle East," in *Proceedings of the SPE Reservoir Characterisation and Simulation Conference and Exhibition*, Abu Dhabi, UAE.

[2] E. Tillero, "Stepping forward: An automated rock type index and a new predictive capillary pressure function for better estimation of permeability and water saturation. Case study, Urdaneta-01 heavy oil reservoir," in *Proceedings of the SPE Latin American and Caribbean Petroleum Engineering Conference 2012, LACPEC 2012*, pp. 134–153, Mexico, April 2012.

[3] B. Ji, P. Lian, X. Tan, and T. Duan, "Integrated numerical simulation for a giant, asphaltene riched, carbonate reservoir," in *Proceedings of the SPE Reservoir Characterisation and Simulation Conference and Exhibition, RCSC 2015*, pp. 655–672, UAE, September 2015.

[4] J. Betancourt, "Rock type modeling: An effective method to determine reservoir quality rock to discretize net pay in Lower Guadalupe Formation, Abanico Field Colombia," in *Proceedings of the SPE Latin American and Caribbean Petroleum Engineering Conference 2012, LACPEC 2012*, pp. 532–541, Mexico, April 2012.

[5] N. F. Alhashmi, K. Torres, M. Faisal et al., "Rock typing classification and hydraulic flow units definition of one of the most prolific carbonate reservoir in the onshore Abu Dhabi," in *Proceedings of the SPE Annual Technical Conference and Exhibition, ATCE 2016*, UAE, September 2016.

[6] A. L. M. Compan, G. C. R. Bodstein, and P. Couto, "A relative permeability rock-typing methodology with a clustering method combined with a heuristic optimization procedure," *SPE Journal*, vol. 21, no. 5, pp. 1899–1915, 2016.

[7] F. Ben Amor, Z. Kindi, S. Kriplani, A. Panda, C. Darous, and A. H. Akram, "An Innovative Approach for Integrated Characterization and Modeling of a Complex Carbonate Reservoir," in *Proceedings of the SPE Middle East Oil & Gas Show and Conference*, Manama, Kingdom of Bahrain.

[8] S. A. Purba, A. P. Garcia, and Z. Heidari, "New Method for Rock Classification in Carbonate Formations Using Well-Log-Based Rock Fabric Quantification," in *Proceedings of the SPWLA 58th Annual Logging Symposium*, Oklahoma, USA, 2017.

[9] M. Tariq, P. Bizarro, A. De Sousa, and M. T. Ribeiro, "Reservoir characterization and modeling of a carbonate reservoir - Case study," in *Proceedings of the Abu Dhabi International Petroleum Exhibition and Conference 2012 - Sustainable Energy Growth: People, Responsibility, and Innovation, ADIPEC 2012*, pp. 728–745, UAE, November 2012.

[10] C. Hollis, V. Vahrenkamp, S. Tull, A. Mookerjee, C. Taberner, and Y. Huang, "Pore system characterisation in heterogeneous carbonates: An alternative approach to widely-used rock-typing methodologies," *Marine and Petroleum Geology*, vol. 27, no. 4, pp. 772–793, 2010.

[11] X. Tan, P. Lian, J. Zhang et al., "A new method for 3D oil reservoir modeling based on "double seismic constraint," *Shiyou Xuebao/Acta Petrolei Sinica*, vol. 37, no. 12, pp. 1518–1527, 2016.

[12] N. El-Khatib, "Development of a Modified Capillary Pressure J-Function," in *Proceedings of the Middle East Oil Show*, Bahrain.

[13] H. Saboorian Jooybari, G. H. Mowazi, and S. R. Jaberi, "A new appoach for rock typing used in one of the Iranian carbonate reservoir (a case study)," in *Proceedings of the International Oil and Gas Conference and Exhibition in China 2010: Opportunities and Challenges in a Volatile Environment, IOGCEC*, pp. 2626–2635, China, June 2010.

[14] S. Kolodzie, "Analysis of pore throat size and use of the Waxman-Smits equation to determine OOIP in Spindle field. Colorado," *Society of Petroleum Engineers of AIME, (Paper) SPE*, 2017.

[15] J. O. Amaefule, M. Altunbay, D. Tiab, D. G. Kersey, and D. K. Keelan, "Enhanced reservoir description: using core and log data to identify hydraulic (flow) units and predict permeability in uncored intervals/wells," in *Proceedings of the SPE Annual Technical Conference and Exhibition. Part 2(of 5)*, pp. 205–220, October 1993.

[16] M. Abbaszadeh, H. Fujii, and F. Fujimoto, "Permeability prediction by hydraulic flow units - Theory and applications," *SPE Formation Evaluation*, vol. 11, no. 4, pp. 263–271, 1996.

[17] D. G. Hatzignatiou, Y. Zhou, and J. O. Helland, "A dimensionless capillary pressure function for imbibition derived from pore-scale modeling in mixed-wet rock images," in *Proceedings of the SPE Improved Oil Recovery Symposium*, Tulsa, Oklahoma, USA.

[18] O. Jin, I. Saeed, F. Mohammad, P. Tian, I. Mostafa, and M. A. Chughtai, "Dynamic rock typing study of a complex heterogeneous carbonate reservoir in oil field, Iraq," in *Proceedings of the Abu Dhabi International Petroleum Exhibition and Conference, ADIPEC 2016*, UAE, November 2016.